PREPRINT UCRL-76961

ONF-750734--1

# Lawrence Livermore Laboratory

MAGNETOHYDRODYNAMICS NEAR A BLACK HOLE

James R. Wilson

August 14, 1975

This paper was prepared for submittal to the Proceedings of Marcel Grossman Meeting on the Recent Progress of the Fundamentals of General Relativity Miramare - Trieste, Italy, July 7-12, 1975.



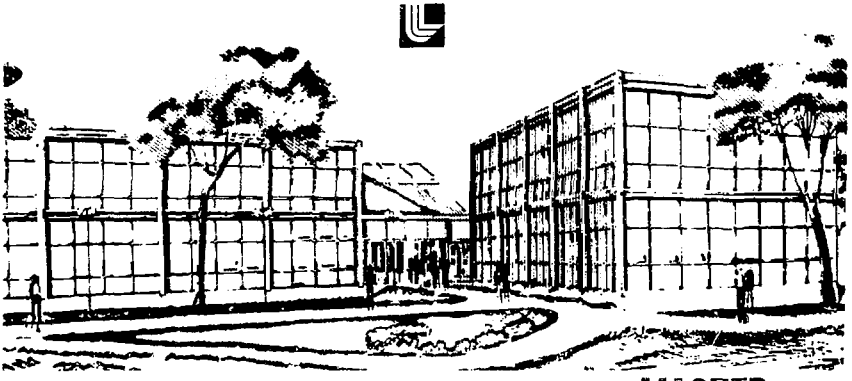

# MAGNETOHYDRODYNAMICS NEAR A BLACK HOLE*

James R. Wilson

Lawrence Livermore Laboratory, University of California

Livermore, California 94550

## I. INTRODUCTION

We present in this paper a numerical computer study of hydromagnetic flow near a black hole. First, the equations of motion are developed to a form suitable for numerical computations. Second, the results of calculations describing the magnetic torques exerted by a rotating black hole on a surrounding magnetic plasma and the electric charge that is induced on the surface of the black hole are presented.

## II. THE EQUATIONS

We start from the divergence of the energy momentum tensor for a perfect fluid

$$T^{\nu}_{\mu;\nu} = \frac{1}{\sqrt{-g}} \frac{\partial}{\partial x^{\nu}} (T^{\nu}_{\mu} \sqrt{-g}) + \frac{1}{2} \frac{\partial g^{\alpha\beta}}{\partial x^{\mu}} T_{\alpha\beta} \qquad (1)$$

where

$$T_{\mu\nu} = (\rho + \epsilon + P) U_{\mu} U_{\nu} + g_{\mu\nu} P. \qquad (2)$$

*This work was performed under the auspices of the U. S. Energy Research & Development Administration.

To put this in a form suitable for computations, a momentum density $S_\mu = (\rho + \epsilon + P)U_\mu U^t$, a time four velocity $V^\mu = U^\mu U^t$, and a number density $D = \rho U^t$ are introduced, where $\rho$ is the proper number density of the fluid, $\epsilon$ is the proper thermal energy density, $P$ is the pressure, and $U^\mu$ is the usual four velocity.

With manipulation, the energy and particle conservation equations become

$$\frac{1}{\sqrt{-g}} \frac{\partial}{\partial x^\nu} (S_\mu V^\nu \sqrt{-g}) + \frac{\partial P}{\partial x^\mu} + \frac{1}{2} \frac{\partial g^{\alpha\beta}}{\partial x^\mu} \frac{S_\alpha S_\beta}{S^t} = 0 \tag{3}$$

and

$$\frac{1}{\sqrt{-g}} \frac{\partial}{\partial x^\nu} (D V^\nu \sqrt{-g}) = 0. \tag{4}$$

While these equations are sufficient to determine hydrodynamic flow, it is preferable to use only the three space-like momentum elements of Eq. (3) and the time-projected part of $T^\mu_{\nu;\mu}$ to find the time behavior of $\epsilon$.

Consider $U^\nu T^\mu_{\nu;\mu} = 0$. Then, using the condition $U^\nu U_\nu + 1 = 0$ to evaluate and simplify the divergence terms, and introducing an energy density $E = \epsilon U^t$, the energy equation becomes:

$$\frac{\partial}{\partial x^\mu} (E V^\mu \sqrt{-g}) + P \frac{\partial}{\partial x^\mu} (U^t V^\mu \sqrt{-g}) = 0. \tag{5}$$

These equations have now been made as similar as possible to the Newtonian Eulerian hydrodynamic equations, for which a large body of numerical methodologies exist.

Next, we add the equations for the magnetic fields. At the start we specialize to axial symmetry. The magnetic field is described by two

independent variables: $H_\phi$, the component of the magnetic field about the axis of symmetry; and $A_\phi$, the vector potential component about the symmetry axis. Consider the plasma as a perfect conductor expressed by setting the comoving electric field $U^\mu F_{\mu\nu}$ equal to zero, where $F_{\mu\nu}$ is the electromagnetic field tensor. With the condition of a zero electric field the components of the electromagnetic tensor are

$$F_{RZ} = H_\phi, \quad F_{R\phi} = \frac{\partial A_\phi}{\partial R}, \quad F_{Z\phi} = \frac{\partial A_\phi}{\partial Z}, \tag{6}$$

$$F_{tZ} = V^\phi F_{Z\phi} - V^R F_{RZ}, \quad F_{tR} = V^\phi F_{R\phi} + V^Z F_{RZ},$$

and

$$F_{t\phi} = -V^R F_{R\phi} - V^Z F_{Z\phi}.$$

This last equation can be reinterpreted as the time-evolution equation for the vector field component $A_\phi$

$$\frac{\partial A_\phi}{\partial t} = -V^R \frac{\partial A_\phi}{\partial R} - V^Z \frac{\partial A_\phi}{\partial Z}. \tag{7}$$

The time evolution of $H_\phi$ is found from the Maxwell equation $F_{\mu\nu;\eta} + F_{\eta\mu;\nu} + F_{\nu\eta;\mu} = 0$, with $\mu = R$, $\nu = Z$, $\eta = t$. (Other components of the equation are solved identically by choosing $A_\phi$ and $H_\phi$ to describe the magnetic field.)

The equation for $H_\phi$ is

$$\frac{\partial H_\phi}{\partial t} = \frac{\partial}{\partial Z}\left(V^\phi \frac{\partial A_\phi}{\partial R} - V^Z H_\phi\right) - \frac{\partial}{\partial R}\left(V^\phi \frac{\partial A_\phi}{\partial Z} - V^R H_\phi\right). \tag{8}$$

Finally, the electromagnetic force $F_{\mu\nu} J^\nu$ must be added to the momentum equation where $J^\nu = \frac{1}{\sqrt{-g}} \frac{\partial}{\partial x^\mu} (F^{\mu\nu}\sqrt{-g})$ is the electric current.

Because the plasma is a perfect conductor, no additional terms occur in the energy equation.

In the rest of the paper we are concerned only with a static metric. To recapitulate, the equations in this situation are

$$\frac{\partial D}{\partial t} + \frac{1}{\sqrt{-g}} \frac{\partial}{\partial x^i} (\sqrt{-g} V^i D) = 0 \qquad \begin{matrix} i & R, Z \\ j & R, Z, \phi \end{matrix} \tag{9}$$

$$\frac{\partial E}{\partial t} + \frac{1}{\sqrt{-g}} \frac{\partial}{\partial x^i} (\sqrt{-g} V^i E) + P \left[ \frac{\partial U^t}{\partial t} + \frac{1}{\sqrt{-g}} \frac{\partial}{\partial x^i} (\sqrt{-g} V^i U^t) \right] = 0$$

$$\frac{\partial S_j}{\partial t} + \frac{1}{\sqrt{-g}} \frac{\partial}{\partial x^i} (S_j V^i \sqrt{-g}) + \frac{\partial P}{\partial x^j} + \frac{1}{2} \frac{\partial g^{\alpha\beta}}{\partial x^j} \frac{S_\alpha S_\beta}{S^t} = J^F F_{tj} = 0$$

$$\frac{\partial H_\phi}{\partial t} = \frac{\partial H_\phi}{\partial Z} \left( V^\phi \frac{\partial A_\phi}{\partial R} - V^Z H_\phi \right) - \frac{\partial}{\partial R} \left( V^\phi \frac{\partial A_\phi}{\partial Z} + V^R H_\phi \right)$$

$$\frac{\partial A_\phi}{\partial t} = - V^R \frac{\partial A_\phi}{\partial R} - V^Z \frac{\partial A_\phi}{\partial Z} .$$

The $V^i$ are found from $S_j$, D, and E by using the velocity normalization condition $U^\mu U_\mu + 1 = 0$. A perfect gas equation-of-state with an adiabatic coefficient of 1.5 completes the hydrodynamic description of the system. A coefficient of 1.5 was chosen because the electrons are completely relativistic while the ions are weakly relativistic at the level where shock waves are formed.

We use the Boyer-Lindquist form of the Kerr metric expressed in cylindrical R, Z coordinates.

have any discernable effect on the plasma flow. A calculation was also performed with counter-rotating plasma a = 1, A = -4, and H = 0.01. Even with these large values of A and H, the plasma flowed smoothly, though not straight into the hole. No shock wave was formed.

## SUMMARY

We looked at very specialized cases of accretion onto a black hole and noted two main effects: the induction of charge on a black hole and the extraction of energy from rotating black holes by the magnetic rigidity. At present it is hard to see what observable effects these processes have. At the moment, the interest is mostly in principle. What is needed is an analysis of the fields to see if they grow into catastrophically magnetohydrodynamically unstable configurations, and thus produce short bursts of high-energy particles. There is a tendency to form current sheets and concomitant charge sheets on the equator. In the present calculations there is also a build up of density along the equator, which argues against any sudden release of field energy near the waist by, say, field reconnection, because inertial effects would dampen it. When a shock develops, the density near the equator builds up almost an order of magnitude above free-fall density. We might envisage material falling in smoothly with a simple field configuration, building up a complicated field near the hole, and extracting some energy from the hole. It would then become very unstable, releasing a lot of field energy and allowing the material stacked near the hole to fall in. The whole process would then repeat itself. This is very speculative.

$$g^{RR} = \frac{\Delta}{\rho^2}\left(\frac{Z^2}{\Delta} + \frac{R^2}{r^2}\right); \quad g^{RZ} = \frac{RZ}{\rho^2}\left(\frac{\Delta}{r^2} - 1\right); \quad g^{ZZ} = \frac{\Delta}{\rho^2}\left(\frac{R^2}{\rho^2} - \frac{Z^2}{r^2}\right) \tag{10}$$

$$g^{\phi\phi} = \frac{r^2}{\rho^2 R^2} - \frac{a^2}{\rho^2 \Delta}; \quad g^{\phi t} = \frac{2amr}{\rho^2 \Delta}; \quad g^{tt} = -\left[1 + \frac{2mr(a^2 + r^2)}{\rho^2 \Delta}\right]; \quad \sqrt{-g} = \frac{R\rho^2}{r^2},$$

where $r^2 = R^2 - Z^2$, $\rho^2 = r^2 + a^2 Z^2/r^2$, $\Delta = r^2 - 2mr + a^2$, m is the hole mass, and a is the hole angular momentum.

To solve these differential equations, a finite, rectangular mesh is set up in R, Z space. The variables $S_j$, $A_\phi$, and $V_i$ are considered to be centered at the mesh corners. The variables D, E, P, $H_o$, and $g^{\alpha\beta}$ are thought to be centered between the mesh corners (Fig. 1). The grid is drawn for a = 0 so that 20 equal zones span the hole in each direction. Ten zones span the hole for a = 1. Outside the hole, zone size increases by a constant factor zone-to-zone so that the outside boundary is 10 times the hole radius. Forty zones span each direction. See Fig. 2 for overall calculational grid.

Many methods exist in the literature of numerical techniques for solving these equations. Several second-order schemes were tried, but were found to give very poor results near the horizon of the hole because of sharp changes in the variables from one zone to the next. The scheme adopted is about the simplest. In convection terms such as $\frac{1}{\sqrt{-g}}\frac{\partial}{\partial x^i}(D V^i \sqrt{-g})$, the flux of mass in the Z direction across a zone boundary is represented by $D_b (V^i_{K,J} - V_{K,J+1}) \cdot (\sqrt{-g}_{K,J} + \sqrt{-g}_{K-1,J}) \cdot (R_{J+1} - R_J)/4$.

Where $D_b$ is the density in the zone behind the zone boundary with respect to the velocity, i.e., if $V_{K,J} + V_{K,J+1}$ is greater than zero, $D_b = D_{K-1,J}$, otherwise $D_b = D_{K,J}$. In all but convection terms, straight arithmetic averages are used to make all terms in any equation center at

the same point in space. The non-transport part of the momentum equation is time-centered one-half time-step from the transport-type equations. Pressure in the energy equation is time-centered with respect to the new and old energies, otherwise all equations use old values to compute the new values. An artificial viscosity, or Richtmyer-Von Neumann dissipation pressure is introduced to provide the correct entropy change in shock waves. Dissipation pressure is

$$Q = D\left[\left(\Delta_R V^R\right)^2 + \left(\Delta_Z V^Z\right)^2\right],$$

$\Delta_R V^R$ is the change in R velocity across a zone in the R direction. Here, $Q$ is equal to zero unless $\frac{\partial \rho}{\partial t} > 0$ and $\Delta_R V^R < 0$ or $\Delta_Z V^Z < 0$. The $Q$ pressure is added to the $P$ pressure everywhere that $P$ occurs in the equations of motion.

We made test calculations to study the accuracy of the shock calculations in flat space. The error in shock compression was about 5% for nonrelativistic shocks and rose to about 20% for a shock velocity of 0.995, which is much higher than encountered in these calculations. Shock waves form a few black hole radii out, and hence the velocities are about one-half to one-third of light velocity.

The metric is singular on the horizon because the $\Delta$ term disappears on the horizon. Numerical problems very close to the horizon are avoided when a minimum of 0.025 $m^2$ is placed on $\Delta$. This allows material to actually fall into the hole. The self-gravitational effects of the plasmas are assumed to be negligible.

A test calculation was also made for material free-falling into a Schwarzchild hole with no internal, rotational, or magnetic energy. The

magnitude of the velocities was good, but the directions were inclined slightly from the 45° line toward the equator and the axis. Just outside the horizon, the density at the waist and axis was 2 to 3 times the density at 45°. The density along the 45° line is very close to the true solution. If the present simple differencing scheme is used in a Newtonian calculation, the same divergence toward the waist and axis is observed. This is because the zones are not square. In the Newtonian calculation this divergence can be eliminated by higher order corrections. However, these more complicated difference methods, when used with the relativistic equations, are unstable near the horizon. Although a density factor of three may seem large, the density of free-fall, pressureless gas varies as

$$D \approx 1\, r^{3.2}\, (1 - 2m\, r),$$

so that it diverges at the horizon. Also, the value of $S_t$ near the horizon rises about three to six times that of the true solution in these calculations. In this case $S_t$ varies in the same manner as $D$, however $S_t$ is found by the velocity renormalization condition, and the momentum density varies as

$$S_r \cong 1\, (r - 2m)^2.$$

Indirectly, $S_t$ is more divergent than $D$ near the horizon. (Most of the interesting action in the following calculations occurs a few hole radii from the hole so that large errors close to the horizon will hopefully not overly affect the results.) A too large $S_t$ increases the inward gravitational forces relative to the centrifugal and magnetic forces.

## III. EXAMPLE CALCULATIONS

For these calculations, a grid mesh is set up in an R, Z space extending from zero to about 10 to 20 times the gravitational radius, m(G = c = 1). Material is introduced at the outer boundary with a density and an R, Z velocity that uniform, cold, nonrotating material falling from infinity would have.

$$D = 1/\left[r\sqrt{2mr}\,(1 - 2m/r)\right],$$

$$S_R = -R/\left[r^3(1 - 2m/r)^2\right],\quad S_Z = -Z/\left[r^3(1 - 2m/r)^2\right]$$

The magnetic field and angular momentum about the Z axis are added to this cold material. The boundary is far enough from the origin, and the added fields and angular momentum are small enough so that if the material had fallen from infinity with those values of magnetic flux and angular momentum, the flow would have been only slightly affected. These boundary conditions are rather specialized, but they could represent the inside flow in black hole accretion from a solar wind. The range of angular momentum values considered here may be too low for most real astronomical situations, i.e., disk accretion. A main reason for considering this type of accretion is that it develops quickly on the characteristic hydrodynamic time scale.

It may be useful to consider a few elementary, relevant facts of orbits about a black hole (Bardeen, Press, and Teukolsky, 1972).[1] In a *Schwartzchild metric*, the minimum radius and minimum specific angular momentum for stable circular orbits in the equator are 6 m and $2\sqrt{3m}$,

respectively. Angular momentum values in the examples are always less than the above values so that material cannot be stopped by rotation alone. However, the shear in angular velocity produces large toroidal ($H_\phi$) fields from an initial poloidal field ($H_R$, $H_Z$). If enough field pressure is developed this way, material is slowed sufficiently to produce a shock wave, even with relatively low angular momentum. In an extreme Kerr metric, the last stable circular orbit is at the horizon and has an angular momentum of only $2\sqrt{3}$. Even without angular momentum, particles rotate about a Kerr hole and, if any poloidal field is present, the total magnetic field is strongly amplified and retards the inward flow. Also, relatively small angular momentum (of the order of unity) will affect the flow if the plasma is corotating with an extreme Kerr hole. The dragging of inertial frames in the Kerr metric can be thought of as adding Coriolis force $\omega U_\rho / R$ where $\omega$ is the angular velocity of the inertial frame.

The calculations are limited by three variables: a, the angular momentum of the black hole, (henceforth the mass m of the hole will be taken as one); A, the specific angular momentum of the infalling gas at the equator boundary; and, H, the ratio of magnetic field energy density to Plasma mass density at the boundary. The magnetic field at the boundary is taken as totally poloidal. It is dominantly an $H_Z$ field along the cylindrical boundary. Because the density decreases along the cylindrical boundary going from the equator, the field intensity also decreases; the field is not strictly an $H_Z$ field. All points not on the equator are given an angular momentum of $A(R/R_e)$ where $R_e$ is the cylindrical radius at the equator. The average angular momentum per unit mass is approximately 5/6 of the nominal value A, because the

outside of the calculational mesh is usually square. Calculations are symmetric with respect to the equator, $Z = 0$, plane.

In a previous paper (Wilson 1971)[2] similar calculations were made for the case of no magnetic field. For in-fall into a Schwartzchild hole, very large angular momentum was needed to alter the flow from smooth adiabatic infall. Even a large angular momentum of $A = 4$ formed only a weak shock wave, and it arose primarily from the material colliding at the equator. The centrifugal force deflects the material from straight in the equator. To really stop material it is probably necessary to use an $A$ appreciably greater than $2\sqrt{3}$, the value of angular momentum for the last stable orbit around a Schwartzchild hole. When the material slows down in a shock wave, for example, it acquires more energy per particle, but does not change its angular momentum. It decreases its angular momentum and falls inside the radius of the last stable orbit, even though it began with an angular momentum greater than the angular momentum of the last stable orbit. It can also be pushed into the hole by fluid thermal pressures. Kerr hole calculations with $a = 0.7$, $A = 3$ and $a = 1$, $A = 2$ were marginal for the development of a shocked region. With $a = 1$, $A = 3$ a strong clear shock developed in the waist region, forming a hot toroidal doughnut of gas in the equatorial region. The internal energy was about 0.1 when the shock region radius had grown to about 8. The radius of the shocked region grew with a velocity of about 0.1 until the shock wave was out to about 10. Whether it slows down at some moderately small radius or keeps growing outward indefinitely is not known. With $a = 1$, $A = -4$ the centrifugal forces were large far out, and strongly deflected the material

toward the waist. In close, the lessening of the centrifugal force by antirotation pulled so strongly on the material that no shock waves were formed. In general, pure hydrodynamic flows tend to be simple.

The first calculation is for free fall into a Schwartzchild hole with a very low angular momentum and magnetic field (a = 0, A = 0.0001, and H = 0.0001). The flow is only slightly perturbed from spherical infall. However, enough field and nonradial flow is produced to induce a small electric charge on the hole. The electric charge is given by $e = 2A_\phi^o$ A where $A_\phi^o$ is the vector potential on the equator of the hole and equal to the magnetic moment of the hole. Figure 3 shows the magnetic field structure at 90. The poloidal field lines tend toward a radial field configuration, but the field lines are not radial because the material with field in it has only been falling in for a finite time. Also, the field started at a radius of 20 (with the configuration described in the last paragraph) so the field will never become strictly radial. In a radial field, a current sheet forms on the equator. In this calculation the current is concentrated near the equator. The electric charge density is likewise concentrated in the equator region. The electric field lines could be thought of as arising mostly from the horizon of the hole and near the equator. Consider an ideal case of a purely radial magnetic field given by $A = A\left(1 - \frac{|Z|}{r}\right)$. The toroidal field can be found easily from Eq. (8) and the free-fall velocity $V^r = \left(1 - \frac{2m}{r}\right)\frac{2m}{r}$:

$$H_\phi = \frac{1}{r^2}\sqrt{\frac{r}{2m}}\, A_o \frac{V\phi(\theta)}{\sin\theta} .$$

In the computer calculations $V_\phi = \sin^2\theta$, for $\theta$ small because of the boundary condition on A. Hence $H_\phi$ is small near the axis in Fig. 3. The smallness of $H_\phi$ near the equator arises because the poloidal field is not radial near the equator. The charge and $A^o_\phi$ are increasing linearly with time. The radial electric field has two terms, $U_\phi H_\theta$ and $U_\theta H_\phi$ ($\theta$ is the spherical polar angle), arising from the condition of perfect conductivity. Breaking the spherical symmetry by either having $H_\theta$ or $U_\theta$ not equal to zero produces a charge. In this low-field, low-rotation example, the charge arises primarily from the $U_\phi H_\theta$ term. If true steady-state accretion exists, with radial infall, the magnetic field would be purely radial and no charge could arise.

The charge on the hole is calculated by the integral of the radial electric field at the inner-most zones over the surface of the hole. Whether the charge belongs to the hole or the infalling gas is obscure. For a star accreting cold material at a rate of $\dot{m}$, the density near the horizon is given by

$$D = \frac{\dot{m}}{8\pi m}\sqrt{\frac{2m}{r}}\ \frac{1}{(r - 2m + 4\dot{m}m)}.$$

Integrating this density out from the horizon to a small fraction of the radius, the mass near the hole is

$$\delta m = 2m\dot{m}\ \log\frac{(r - 2m + 4m\dot{m})}{4m\dot{m}}.$$

Just outside the hole is a moderately large mass with essentially the same mean coordinate density D as the hole density. With the large charge-to-mass ratio of electrons ($2 \times 10^{21}$), this exterior layer can sustain as large

a charge as is interesting. For $\dot{m} = 10^{17}$ g/s, $m = M\odot$, and $\frac{\delta m}{m}$ $= 2.2 \times 10^{-22} \log(r - 2m + 4m\dot{m})/4mm$. Analytical solutions presented elsewhere in the proceedings show that charge can be induced onto black holes by external fields, but these are static, or steady-state, solutions that have had infinite time for the field to penetrate the hole.

For the simple solution of steady radial infall, whose $A_\phi$ is a function of $\theta$ only, $H_\theta = 0$ everywhere. For nonsteady radial flow, $(\partial A_\phi/\partial t) = - V^r(\partial A_\phi/\partial r)$. Since $V^r$ approaches zero at the horizon, $H_\theta$ diverges near the horizon. In steady flow the field lines can be thought of as all lying on top of each other at the horizon. That is, while $H_\theta \cong 0$ up to the horizon, it is singular at the horizon. In the real world the $H_\theta$ just becomes large, of the order of $1/(1 - 2m/r)$, which tends to $1/4\dot{m}$. The magnetic field in a local tetrad has the physical component

$$H_{(\theta)} = \frac{H_\theta}{r^2 \sin^2\theta}\left(1 - \frac{2m}{r}\right)^{1/2}.$$

The ratio of densities $D/H^2_{(\theta)}$ thus tends to a constant value, i.e., it is neither zero nor infinity.

The next calculation uses $a = 0$, $A = 0.0001$, and $H = 0.01$. This magnetic field is large enough to strongly deflect the material from its free-fall motion. Figure 4 shows how the charge and equatorial magnetic flux vary with time. The charge changes sign because both $H_\phi$ and $U_\theta$ are reversing signs near the horizon. The magnetic field configuration is shown in Fig. 5. The velocity vectors are closely parallel to the field lines, and the material is only modestly slowed from its free-fall velocity.

For free-fall into a black hole, the angular velocity

$$V^{\phi} = -\left(1 - \frac{2m}{r}\right) \frac{V_{\phi}}{r^2 \sin^2_{\theta}} .$$

Therefore, if $V_{\phi}$ is a function of angle $\theta$, only the shear

$$\frac{\partial V^{\phi}}{\partial r} = -\frac{2}{r^3}\left(1 - \frac{3m}{r}\right)\frac{V_{\phi}}{\sin^2_{\theta}}$$

reverses sign at a radius of 3 m. In the first calculation the free-fall velocity $V^r$ goes to zero so that the field $H_{\phi}$ does not reverse sign. In the more general case it is not clear how the field grows near the horizon.

In the last Schwarzchild calculation, the rotational momentum is given a value large enough to modestly affect the flow if no field were present.[2] Consider A = 2 and a small value of magnetic field, H = 0.0001. Here, the centrifugal field deflects material to the waist, enhancing the magnetic field. The rotational shear also builds up the $H_{\varphi}$ magnetic field to substantial values. Flow without a magnetic field and with an angular momentum of two forms no shock. However enough additional field generation occurs with this relatively low field to slow the material enough to produce a shock and greatly slow the infall. The field acquires the complicated form shown in Fig. 6. The shock front is at the surface where the poloidal field has kinks. The $H_{\phi}$ field has a steep gradient at a radius of about 6 to 10. The thermal energy behind the shock is about 0.03 units.

Material falling in a Kerr metric experiences a rotational dragging. This dragging is resisted by the rigidity of magnetic fields. This combination of frame dragging and field rigidity leads to the possibility of

extracting energy from the rotating hole. To study this effect in its simplest form, two calculations were run with A = 0, H = 0.01, with a a = 0.7 or 1. With this strong a field, the torque on the infalling gas is quite significant. In Fig. 7, the specific angular momentum averaged over the total mass of material in the calculational grid is plotted as a function of time (the calculational grid extends out to R, Z = 10). Initially, the material in the grid had no magnetic field. The material has to fall from the outside nearly to the horizon before the torques are large enough to have effect. Thus, the angular momentum of the plasma doesn't start to rise until a time of 30. Only in the case of the extreme Kerr is the dragging effect strong. In Fig. 8, the angular velocity of the material and of the inertial frames are compared for the two values of a. The material angular velocity curves result from averaging the angular velocities between 45° and the equator. The speed-up only affects a volume of space rather close to the horizon. When material is corotating with the hole, angular momentum is still transferred out. The dashed line in Fig. 6 shows the net increase of angular momentum for a calculation with a = 1, A = 1, H = 0.0001. Because of the weaker magnetic field, the field takes longer to build to where it can affect the material motions. For Fig. 6, the dashed line was shifted about 100 units in time to the left. This case is more interesting because the fields and momentum forces are large enough to partially stagnate the in-falling material and produce a ring of material around the hole with an augmented angular momentum. Figure 9 shows the isoangular momentum contours as well as the field lines and velocity vectors. Outside the A = 1 contour, $A \cong 1$ except near the axis.

The velocity pattern is very typical of all flows resulting in shock formation. A swirling region is formed several hole-radii out but the inside of the swirl is always falling into the hole because of lack of support. Material at a radius of 2 to 4 has an angular momentum of 2. However, as it slides down field lines to the hole it will lose that angular momentum. The stagnation region continues to grow slowly with time.

Figures 10 and 11 show the time evolution of the electric charge, the toroidal magnetic field, and the vector potential on the hole for the cases a = 1, H = 0.0001, and A = 0 or 1. Very large charges are generated on the scales of the magnetic fields. The plasma has a charge of sign opposite to the hole charge. It is not quite equal because nonradial field lines leave the calculational mesh with some rotational velocity. The charge from the field lines exiting the calculational region is $e \cong \int d\vec{A}\ (\vec{v} \times \vec{H})$, which is small but not negligible. For in-falling material with A = 1, the plasma charge is almost twice the hole charge. The system would be electrically neutral only at very large distances.

Calculations were made for angular momentum A = 2, 3, and 4 in the Kerr metric with a magnetic field parameter of H = 0.0001. The behavior qualitatively is similar to the A = 1 example discussed above. Figure 12 shows the field lines and isotoroidal field contours plotted for a = 1, A = 2, and H = 0.0001. The higher rotation rates simply speeded up the formation of the stagnation region. Calculations with a = 1, A = 2, H = $10^{-5}$ and $10^{-6}$ were also done. The H = $10^{-5}$ behaved similarly to H = $10^{-4}$, just taking more time to develop. A very limited shocked region was formed for H = $10^{-6}$ even after a time of 400. The field did not multiply enough to

have any discernable effect on the plasma flow. A calculation was also performed with counter-rotating plasma a = 1, A = -4, and H = 0.01. Even with these large values of A and H, the plasma flowed smoothly, though not straight into the hole. No shock wave was formed.

## SUMMARY

We looked at very specialized cases of accretion onto a black hole and noted two main effects: the induction of charge on a black hole and the extraction of energy from rotating black holes by the magnetic rigidity. At present it is hard to see what observable effects these processes have. At the moment, the interest is mostly in principle. What is needed is an analysis of the fields to see if they grow into catastrophically magnetohydrodynamically unstable configurations, and thus produce short bursts of high-energy particles. There is a tendency to form current sheets and concomitant charge sheets on the equator. In the present calculations there is also a build up of density along the equator, which argues against any sudden release of field energy near the waist by, say, field reconnection, because inertial effects would dampen it. When a shock develops, the density near the equator builds up almost an order of magnitude above free-fall density. We might envisage material falling in smoothly with a simple field configuration, building up a complicated field near the hole, and extracting some energy from the hole. It would then become very unstable, releasing a lot of field energy and allowing the material stacked near the hole to fall in. The whole process would then repeat itself. This is very speculative.

ACKNOWLEDGMENTS

The author would like to thank R. Hanni, R. Leach, and J. LeBlanc for checking the computer program and making several helpful suggestions.

REFERENCES

1. Bardeen, J. M., Press, W. H., and Teukolsky, S. A., Astrophys. J. 178 347 (1972).
2. Wilson, J. R., Astrophys. J., 173 431 (1972).

FIGURE CAPTIONS

Fig. 1. Mesh for interpreting difference equations. Quantities $S_I$, $V_I$, and $A_\phi$ are centered at intersections of solid lines. Quantities D, E, P, $H_\phi$, and $g^{\alpha\beta}$ are centered as indicated between lines.

Fig. 2. Overall view of mesh used in calculations. Hatched zones are considered as interior to the black hole. Curved lines indicate how magnetic field lines look near the boundary.

Fig. 3. Field configuration for in-fall onto a Schwarzchild hole at a time of 90 with A = 0.0001 and H = 0.0001. Solid lines are poloidal field lines, labels represent flux contained within lines, but scale is arbitrary. Dashed lines are lines of constant $H_\phi$ values. $H_\phi$ differs by a factor of two from one dashed line to the next.

Fig. 4. Charge e on the hole and vector potential $A_\varphi$ on the equator of the hole as functions of time for the example of in-fall onto a Schwarzchild hole with A = 0.0001 and H = 0.01.

Fig. 5. Magnetic field configuration for in-fall to a Schwarzchild hole with A = 0.0001 and H = 0.01. Solid lines are poloidal field contours. Dashed lines are toroidal field contours. $H_\varphi$ differs by a factor of two from one dashed line to the next.

Fig. 6. Magnetic field configuration for in-fall to a Schwarzchild hole with A = 2 and H = 0.0001. Labels are the same as Fig. 4.

Fig. 7. Angular momentum per unit mass averaged over the calculational grid versus time. Dashed curve has been shifted forward in time about 100 units.

Fig. 8. Angular velocity $\Omega$ versus radius. Solid curves are material angular velocity. Dashed curves are frame angular velocity. For the upper curves a = 1 and for the lower curves a = 0.7. In both cases A = 0 and H = 0.01.

Fig. 9. Poloidal field lines for the in-fall of material onto an extreme Kerr metric, a = 1, with A = 1 and H = 0.0001. Closed looping lines are contours of A = 1, 1.4, and 2. Arrows indicate direction of material flow. In the region of high A the magnitudes of the velocity are two to five times less than the length of the vectors would indicate. Also the magnitude of the velocity goes to zero near the hole.

Fig. 10. Hole charge, vector potential at the equator of the hole, and toroidal field near the hole as functions of time for a Kerr metric with a = 1, A = 0, and H = 0.0001. Dashed curve is the negative of the charge in the plasma outside the hole.

Fig. 11. Hole charge, vector potential at the equator of the hole, and toroidal yield near the hole as functions of time for a Kerr metric with a = 1, A = 1, and H = 0.0001.

Fig. 12. Magnetic field configuration at a time of 100 for in-fall onto a Kerr metric with a = 1, A = 2, and H = 0.0001. Solid lines are poloidal field lines, dotted lines are contours of $H_\phi$ differing by factor of two, and the dashed curve is the position of the shock wave.



TAL/lc

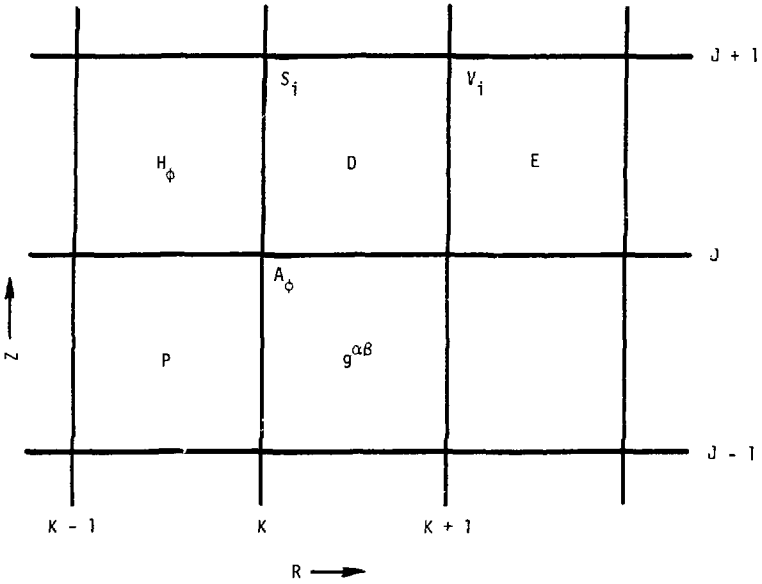


Wilson - Fig. 1

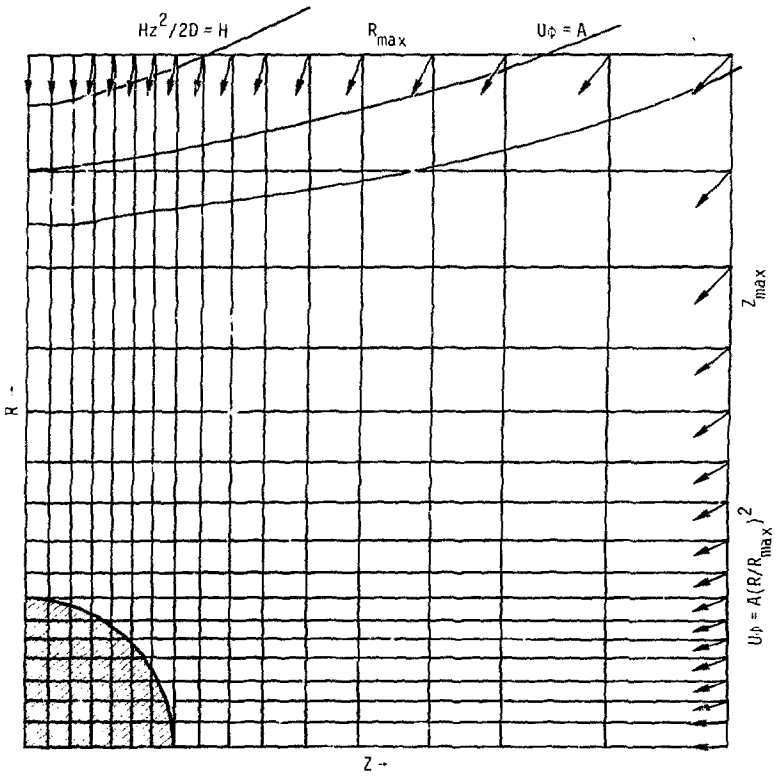


Wilson - Fig. 2

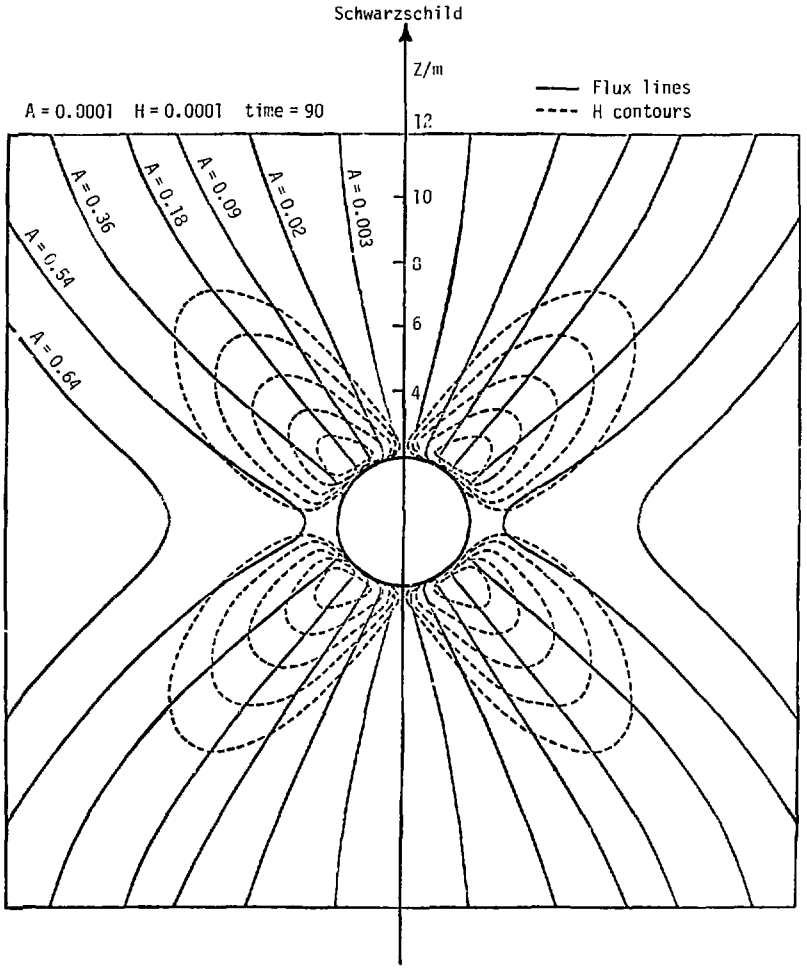
Schwarzschild
Z/m
A = 0.0001 H = 0.0001 time = 90
Flux lines
H contours
12
10
8
6
4
A = 0.36
A = 0.18
A = 0.09
A = 0.02
A = 0.003
A = 0.54
A = 0.64

Wilson - Fig. 3

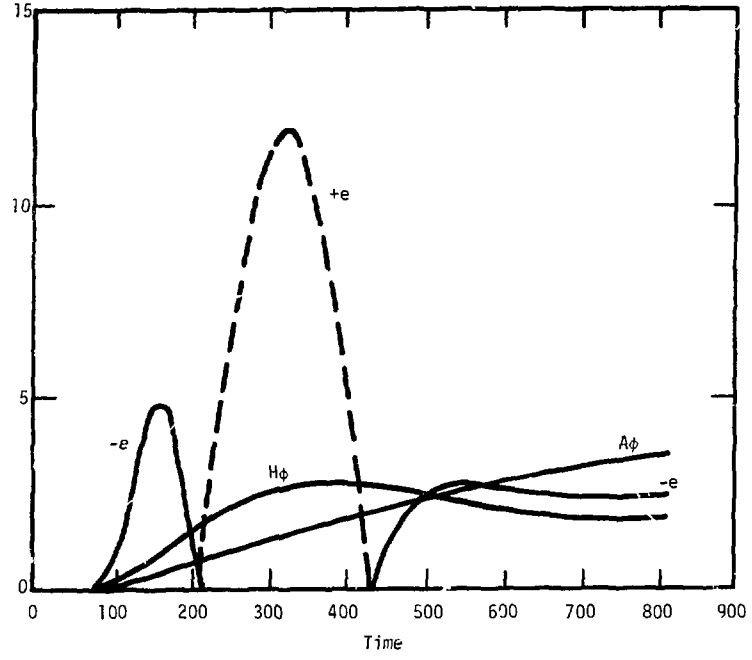


Wilson - Fig. 4

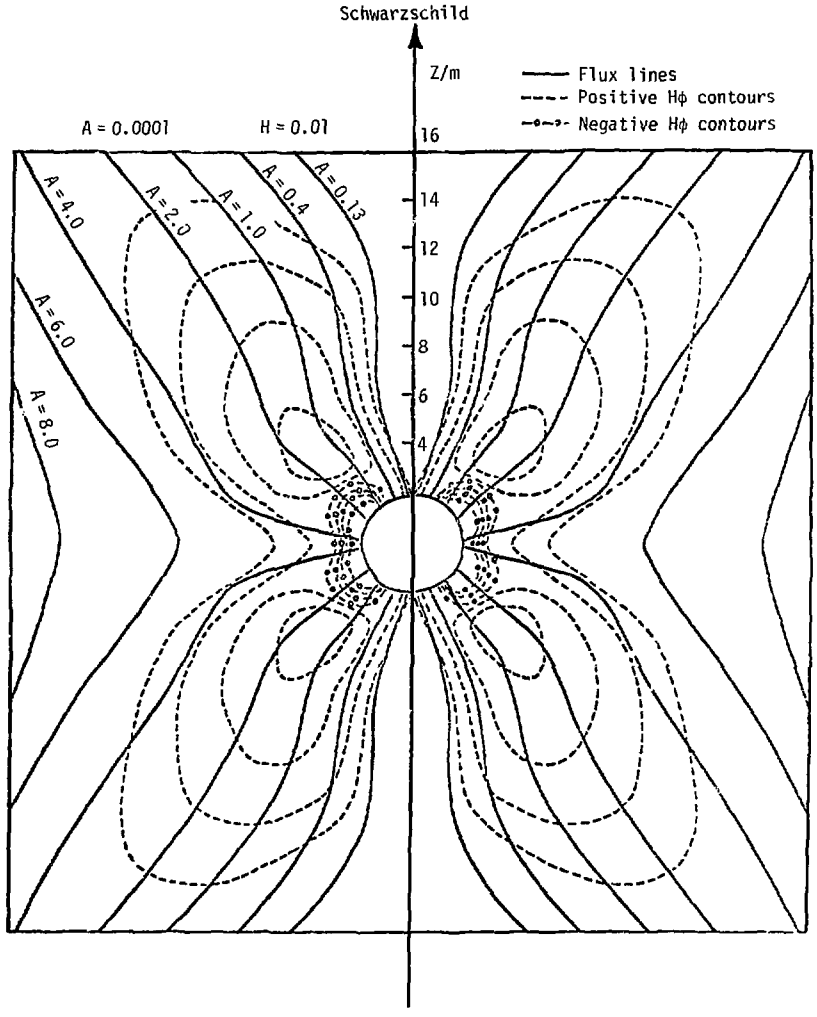
Schwarzschild
Z/m
Flux lines
Positive Hϕ contours
Negative Hϕ contours
A = 0.0001
H = 0.01
16
14
12
10
8
6
4
A=4.0
A=2.0
A=1.0
A=0.4
A=0.13
A=6.0
A=8.0

Wilson - Fig. 5

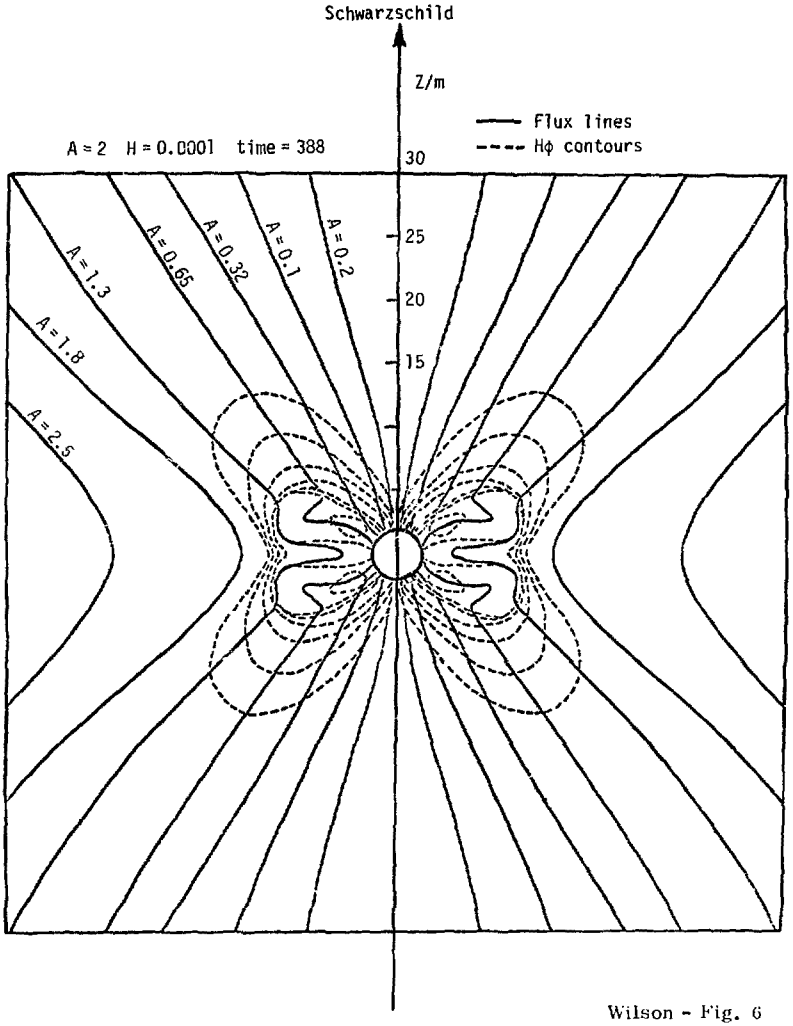
Schwarzschild
Z/m
Flux lines
Hφ contours
A = 2 H = 0.0001 time = 388
30
25
20
15
A=0.2
A=0.1
A=0.32
A=0.65
A=1.3
A=1.8
A=2.5

Wilson - Fig. 6

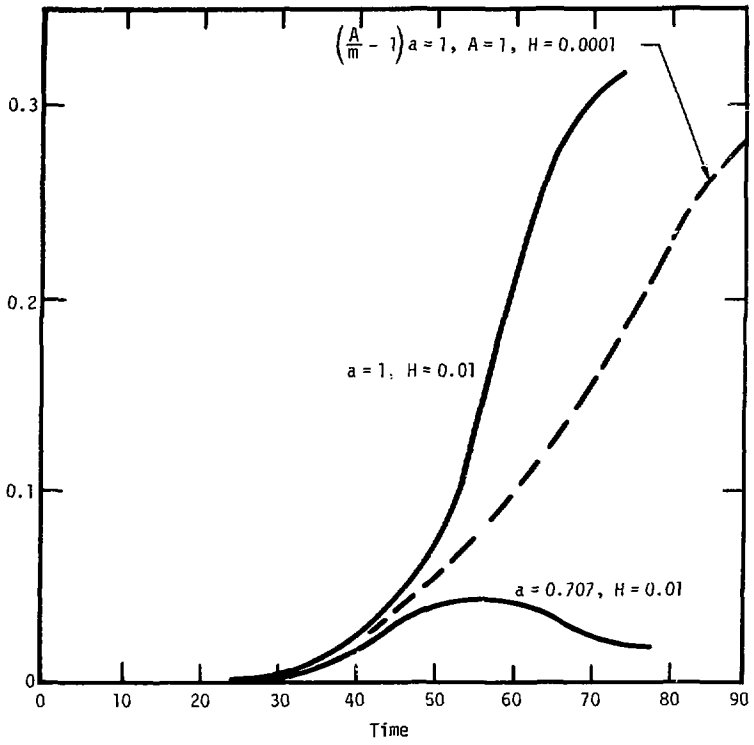
$\left(\frac{A}{m} - 1\right)$ a = 1, A = 1, H = 0.0001
a = 1, H = 0.01
a = 0.707, H = 0.01
0.3
0.2
0.1
0
0
10
20
30
40
50
60
70
80
90
Time

Wilson - Fig. 7

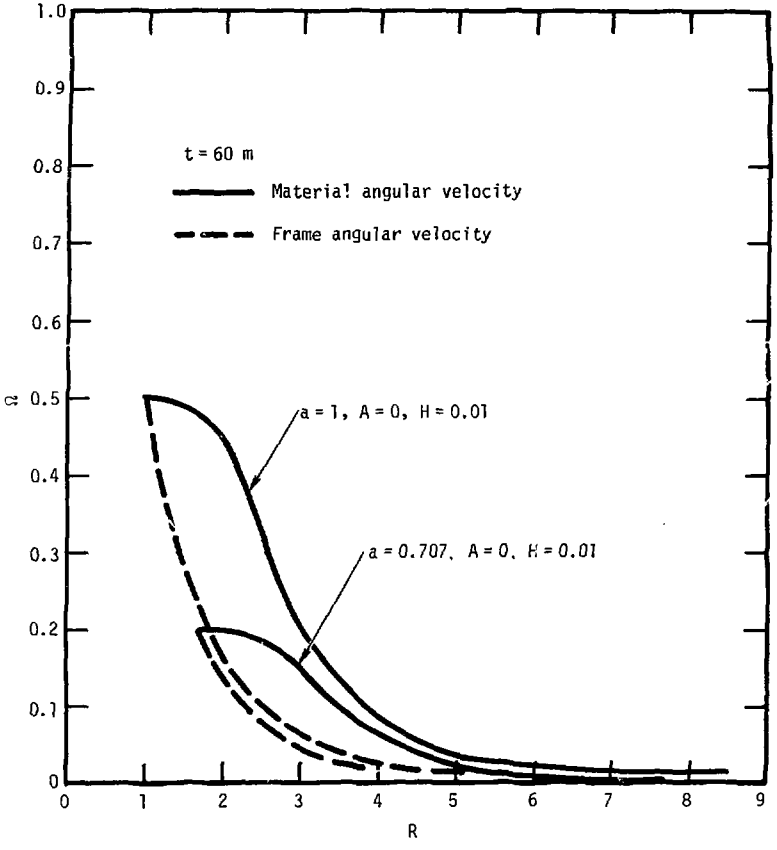
t = 60 m
Material angular velocity
Frame angular velocity
a = 1, A = 0, H = 0.01
a = 0.707, A = 0, H = 0.01
Ω
R
1.0
0.9
0.8
0.7
0.6
0.5
0.4
0.3
0.2
0.1
0
0
1
2
3
4
5
6
7
8
9

Wilson - Fig. 8

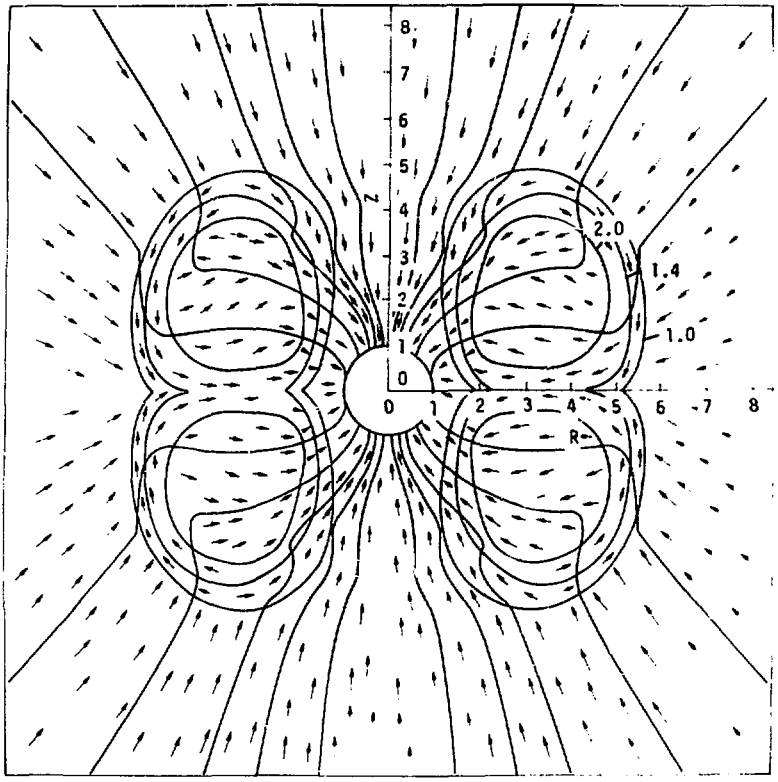


Wilson - Fig. 9

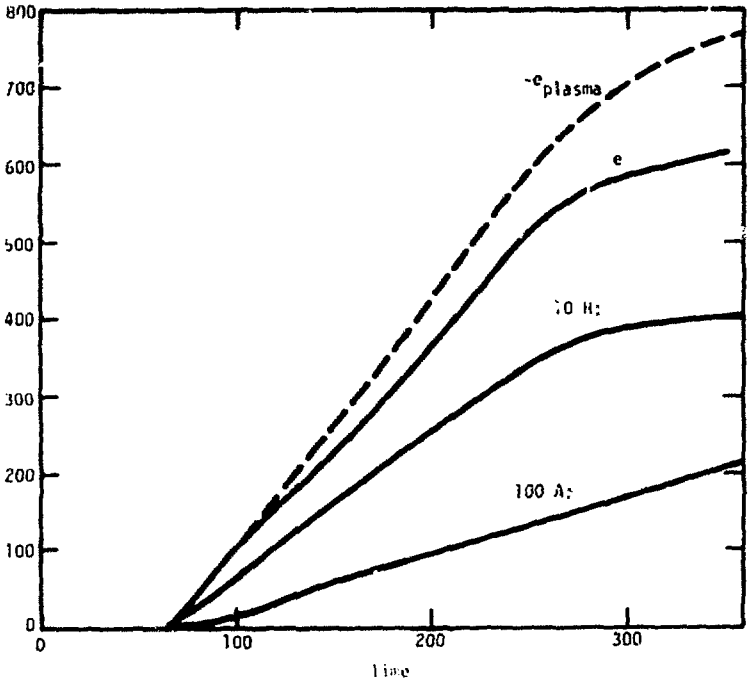


Wilson - Fig. 10

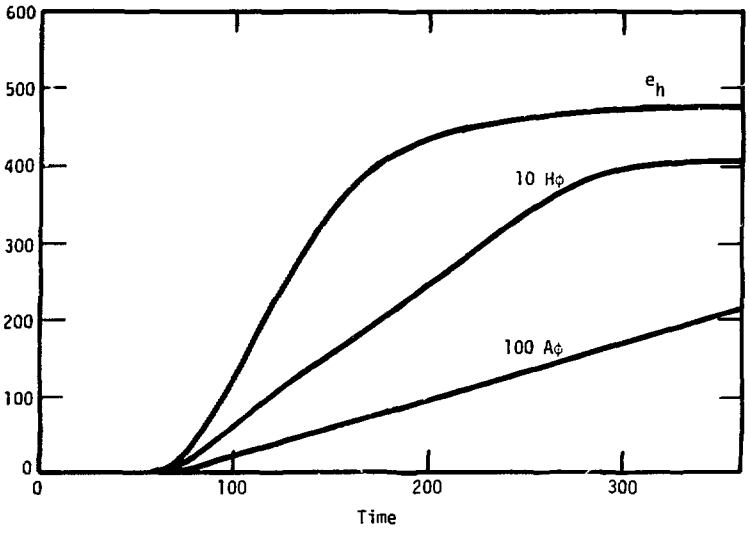


Wilson - Fig. 11

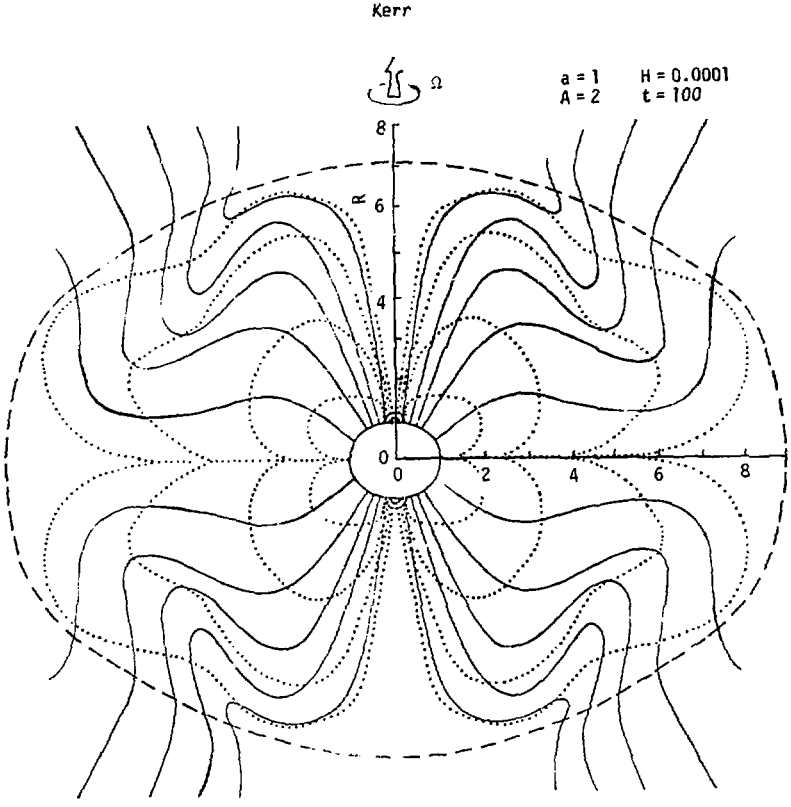


Wilson - Fig. 12